

Reducing Energy Loss and Stabilizing the Perovskite/poly (3-hexylthiophene) Interface through a Polyelectrolyte Interlayer

Wenxiao Zhang, Li Wan, Sheng Fu, Xiaodong Li, and Junfeng Fang*

Experimental Section:

Materials: The SnO₂ colloid precursor and 2, 2, 2-trifluoroethanol (99% +) was obtained from Alfa Aesar (tin (IV) oxide). N,N-dimethylformamide (DMF), and dimethyl sulfoxide (DMSO) were purchased from Sigma-Aldrich. MAI, MABr, MACl, FAI, PbI₂ and Spiro-OMeTAD were purchased from Xi'an Polymer Light Technology Corp. Poly [3-(4-carboxylbutyl)thiophene] (P3CT) and poly(3-hexylthiophene) (P3HT, 4002-E) was purchased from Rieke, America.

Device fabrication: ITO glass was cleaned by sequentially washing with detergent, deionized (DI) water, acetone, and isopropanol (IPA). Before using, the cleaned substrate was dried with N₂ flow and then treated in O₂ plasma for 15 min. Then, the substrate was spin coated with a thin layer of SnO₂ nanoparticle film (1.875%) at 4000 rpm for 30 s, and annealed in ambient air at 150 °C for 30 min. The SnO₂ film was treated in O₂ plasma for 15 min then was transferred to N₂ glovebox. Next, a perovskite film was fabricated through a two-step solution process: the PbI₂ (1.3 M, dissolved in DMF/DMSO (9:1, v/v)) mixed with 5% CsI was spin-coated on ITO/SnO₂ substrate at 2,500 r.p.m. for 30 s and annealed at 70 °C for 1 min in a nitrogen glovebox. After cooling the PbI₂-coated substrate to room temperature in a nitrogen glovebox, a mixed organic cation solution (MAI 0.12 M; MABr 0.05 M; MACl 0.07 M; FAI 0.23 M, dissolved in isopropanol) was spin-coated at 2,300 r.p.m. for 30 s and then annealed at 150 °C for 15 min in air with ~ 40% relative humidity. For thermal stability test, we changed the organic cation solution components (MABr 0.05 M; MACl 0.07 M; FAI 0.35 M, dissolved in isopropanol) to exclude the instability of perovskite layer. The P3CT-BN solution containing P3CT (20 mg) and butylamine (10.9 μl) in 2, 2, 2-trifluoroethanol (1.0 ml) was prepared after dissolving at 60 °C overnight. Then the P3CT-BN solution was diluted to 2 mg/ml for use. The P3HT solution was prepared by dissolving P3HT (20 mg) into mixed solvent (1, 2-dichlorobenzene : diphenyl ether = 97:3 v/v, 1 ml). The Spiro-OMeTAD hole-transport solution was prepared by dissolving Spiro-OMeTAD (72.3 mg), tBP (28.8 μl) and Li-TFSI (17.5 μl, 520 mg ml⁻¹ in acetonitrile) in chlorobenzene (1 ml). For single P3HT HTL based devices, the P3HT solution was spin-

coated on perovskite film at 2000 rpm for 30 s. For P3CT-BN/P3HT based devices, the P3CT-BN solution was deposited on perovskite film at 2000 rpm for 30 s before depositing P3HT layer. For Spiro-OMeTAD based devices, the Spiro-OMeTAD layer was deposited on perovskite by spin-coating at 4000 rpm for 30 s. After depositing HTL, devices fabrication was completed by deposition of an 80 nm patterned Au top electrode by thermal evaporation. All of the abovementioned solutions were filtered through a 0.45 μ m polytetrafluoroethylene filter prior to use.

Characterization:

Photocurrent density-voltage ($J-V$) curves were measured using Keithley 2440 sourcemeter controlled by computer under simulated AM1.5G spectrum (100 mW/cm²) with an Oriel So13A solar simulator. The external quantum efficiency (EQE) measurement was conducted with a Newport quantum efficiency measurement system (ORIEL IQE 200TM) combined with a lock-in amplifier and a 150 W Xe lamp in ambient atmosphere. The light intensity at each wavelength was calibrated by a standard Si/Ge solar cell. Scanning electron microscope (SEM) images were acquired by using a field-emission scanning electron microscopy (Hitachi, S-4800) with an accelerating voltage of 10 kV.

Atomic force microscopy (AFM) (Dimension 3100V, Veeco, tapping mode) was applied to observe the film surface morphology. UV-vis absorption spectrum was recorded on a GS54T spectrophotometer (Shanghai Lengguang Technology Co., China).

X-ray photoelectron spectroscopy (XPS) and ultraviolet photoelectron spectroscopy (UPS) measurements were carried out using Kratos AXIS ULTRA DALD XPS/UPS system. XPS spectroscopy was collected to identify the overall surface composition using a monochromatic Al K α X-ray source (1486.6 eV). UPS measurement was conducted using a HeI (21.2 eV) discharge lamp operated at 20 mA, a pass energy of 5 eV, and a channel width of 25 meV.

Photoluminescence (PL) spectra was analyzed using a fluorescence spectrophotometer (F-4600, Hitachi Ltd., Tokyo, Japan) with a 150 W Xe lamp with excitation wavelength at 466 nm. Time-resolved photoluminescence (TRPL, LabRAM HR800, Horiba Jobin Yvon) decays were conducted with a 532 nm diode laser used as the excitation source. EIS and M-S plot were measured were measured by an electrochemical working station (Solartron Analytical) under 1 sun illumination (AM 1.5) at a reverse potential of 1.2 V at frequencies ranging from 1.0 Hz to 1.0 MHz with oscillation potential amplitudes of 20 mV or at 1 k Hz frequency, respectively.

Stability measurements: Long-term thermal stability is conducted by aging the PSCs on a hot plate at 85

°C in N₂ glovebox or 60 °C in air and the J-V curves are measured after the PSCs cooling down to room temperature. Operational stability of non-encapsulated PSCs is measured through MPP tracking under illumination (100 mW cm⁻², white LED, spectra region: 430-890 nm) at 60 °C using a 16-channel maximum power point MPP measuring system (schematic diagram of the aging setup). During the MPP tracking, the light intensity can be automatic calibrated with a Si reference diode.

Table S1. The device parameters of P3HT based perovskite solar cells.

Device structure	HTL	V_{OC} [V]	J_{SC} [mA cm $^{-2}$]	FF [%]	PCE [%]	Year	Reference
ITO/cp-TiO ₂ /CH ₃ NH ₃ PbI ₃ /P3HT/Ag	pristine P3HT	0.92	17.7	56.2	9.2	2014	[6]
	Li-TFSI+D-TBP doped P3HT	0.98	19.1	66.3	12.4		
FTO/cp-TiO ₂ /mp-Al ₂ O ₃ / CH ₃ NH ₃ PbI _{3-x} Cl _x /HTM/Ag	pristine P3HT	0.92	18.8	61	10.6	2014	[7]
	P3HT/SWNTs-PMMA	1.02	22.7	66	15.3		
FTO/cp-TiO ₂ /cp-TiO ₂ /CH ₃ NH ₃ PbI ₃ /P3HT/Au	pristine P3HT	0.61	16.82	35	3.60	2015	[8]
	BCNs doped P3HT	0.86	17.52	52	8.30		
FTO/cp-TiO ₂ /cp-TiO ₂ /CH ₃ NH ₃ PbI ₃ /P3HT/Au	pristine P3HT	0.946±0.01 (0.932)	17.51±0.77 (18.3)	67.1±1.5 (67.6)	11.11±0.36 (11.53)	2015	[9]
	GD doped P3HT	0.939±0.004 (0.941)	19.63±1.01 (21.7)	71.5±2.3 (71.3)	13.17±0.64 (14.58)		
FTO/cp-TiO ₂ /cp-TiO ₂ /CH ₃ NH ₃ PbI ₃ /P3HT/Ag	pristine P3HT	0.96	16.7	52.6	8.16	2016	[10]
	grapheme doped P3HT	0.99	19.7	70.6	13.82		
FTO/cp-TiO ₂ /mp-TiO ₂ / (FAPbI ₃) _{0.85} (MAPbBr ₃) _{0.15} /P3HT/Au	pristine P3HT	0.96	19.5	55	10.3	2016	[11]
	F4TCNQ doped P3HT	0.97	23.9	62	14.4		
ITO/TiO _x /CH ₃ NH ₃ PbI _{3-x} Cl _x /HTM/Au	P3HT	0.94	20.5	56	10.8	2017	[12]
	PTB7	0.98	22.94	70	15.9		
ITO-PEIE/PCBM/CH ₃ NH ₃ PbI ₃ /P3HT/Au	pristine P3HT	0.868	15.04	47.7	6.23	2017	[13]
	Co(II)-TFSI+tBP doped P3HT	1.06	21.83	70.3	16.28		
FTO/cp-TiO ₂ /mp-TiO ₂ /CH ₃ NH ₃ PbI ₃ /P3HT (MW: 124 kDa)/Au	250 nm mp-TiO ₂	0.984±0.012	15.55±0.73	62.7±0.011	9.59±0.54	2017	[2]
	500 nm mp-TiO ₂	1.024±0.009	23.19±1.20	68.6±0.065	16.27±1.48		

FTO/C60/CsFAPbI ₃ /P3HT/Au	pristine P3HT	~0.9	~20	~50	11-12 (8.7)		2018	[14]
	RGO doped P3HT	~0.9	~20	~60	11-12 (9.8)			
FTO/cp-TiO ₂ /mp-TiO ₂ /CH ₃ NH ₃ PbI ₃ /HTM/Au	pristine P3HT	0.9	18.11	68.6	11.2		2018	[15]
	doped Spiro	1.01	22.15	18.2	17.7			
FTO/cp-TiO ₂ /mp-TiO ₂ /FA _{0.85} MA _{0.15} Pb(I _{0.85} Br _{0.15}) ₃ /P3HT/Au	pristine P3HT	1.024	20.56	67.9	14.30		2018	[16]
	Li-TFSI and tBP doped P3HT	1.072	21.20	77.2	17.55			
	pristine P3HT	0.932±0.02 (0.976)	19.77±0.99 (18.48)	61.69±2.83 (65.92)	11.34±0.46 (11.89)			
FTO/SnO ₂ /CH ₃ NH ₃ PbI ₃ /P3HT/Au	N-CuMe2Pc doped	1.00±0.01 (1.008)	22.09±0.37 (22.44)	70.39±1.95 (73.43)	15.58±0.49 (16.61)		2019	[3]
	pristine P3HT	0.903	16.72	58.0	8.76			
FTO/mp-TiO ₂ /CH ₃ NH ₃ PbI ₃ /P3HT/Au	P3HT:m-MTADATA	0.936	17.34	58.7	9.53		2019	[17]
	Li+tBP doped P3HT	-	-	-	15.62			
(FA _{1-x-y} MA _x Cs _y)Pb(I _{1-x} Br _x) ₃ /P3HT/Au	Li+tBP+Co(III)-TFSI doped P3HT	1.09	23.86	73.7	(14.23±0.44) 19.25		2019	[18]
	P3HT	0.99±0.22	22.51±0.23	62.44±2.27	14.53±0.43 (14.96)			
FTO/cp-TiO ₂ /mp-TiO ₂ /CsFAMA/HTM/MoO ₃ /Ag	PBT1-C	1.03±0.02	22.10±0.27	79.30±1.92	18.6±0.46 (19.06)		2019	[19]
	without WBH	0.925 (R) 0.861 (F)	24.79 (R) 24.68 (F)	69.0 (R) 55.0 (F)	15.8 (R) 11.7 (F)			
FTO/cp-TiO ₂ /mp-TiO ₂ /(FAPbI ₃) _{0.95} (MAPbBr ₃) _{0.05} /P3HT/Au	with WBH	1.145 (R) 1.143 (F)	24.92 (R) 24.92 (F)	79.9 (R) 79.2 (F)	22.8 (R) 22.6 (F)		2019	[1]

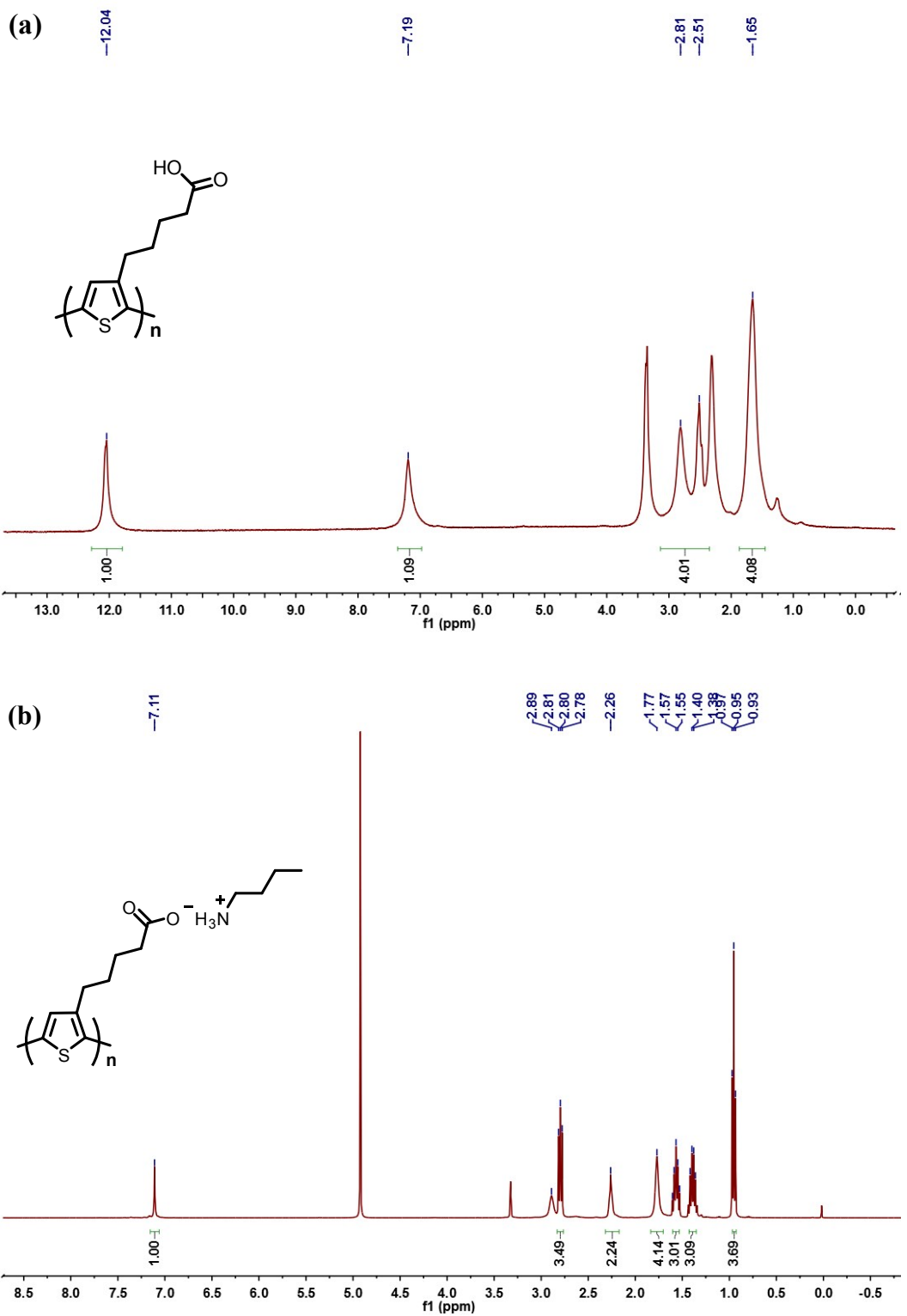


Figure S1. (a) The ^1H NMR spectrum of P3CT in $(\text{CD}_3)_2\text{SO}$ and (b) the ^1H NMR spectrum of P3CT-BN in CD_3OD .

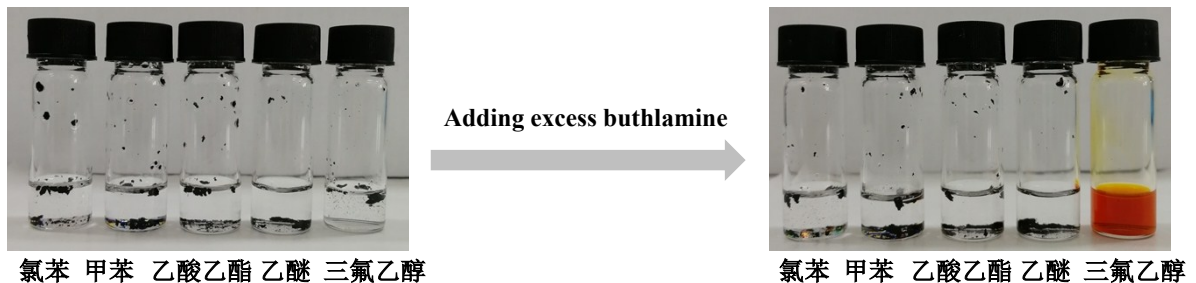


Figure S2. The solubility of P3CT and P3CT-BN in the traditional orthogonal solvents of perovskite.

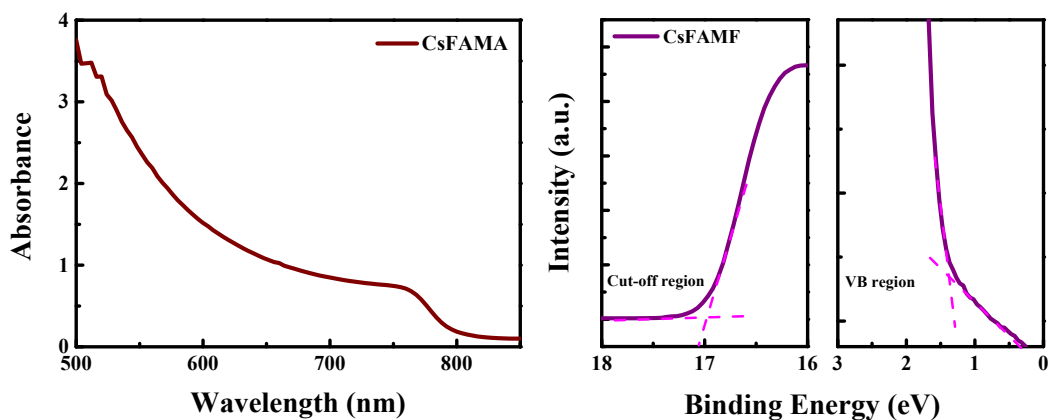


Figure S3. (a) Ultraviolet-visible absorption spectra of CsFAMA perovskite film. (b) Ultraviolet photoelectron spectroscopy (UPS) spectra of perovskite films: secondary electron cut-off region (left) and valence band (VB) region (right).

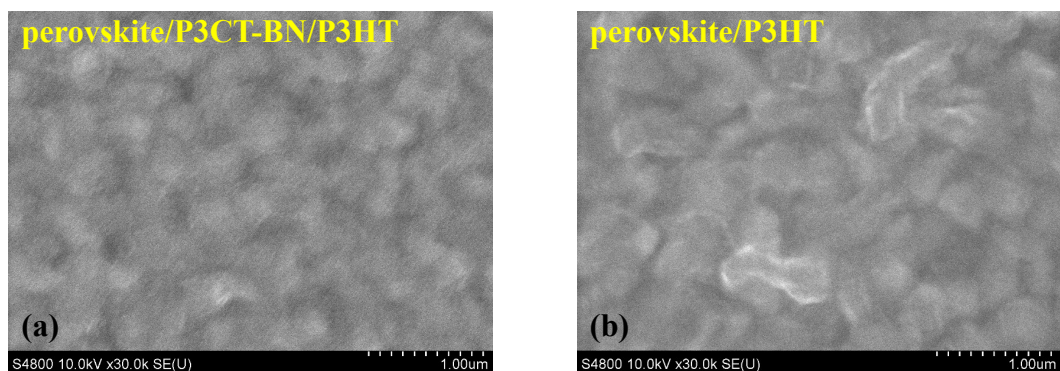


Figure S4. Top-view SEM images of P3HT film deposited on perovskite with (a) and without (b) P3CT-BN interlayer.

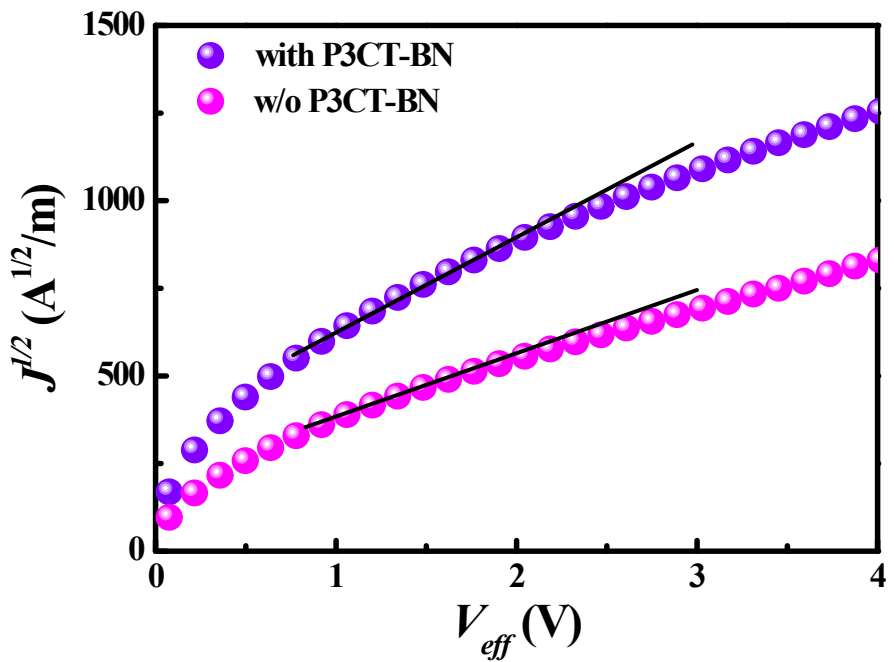


Figure S5. J - V plots of the hole-only devices based on pristine P3HT and P3CT-BN/P3HT bilayer HTMs.

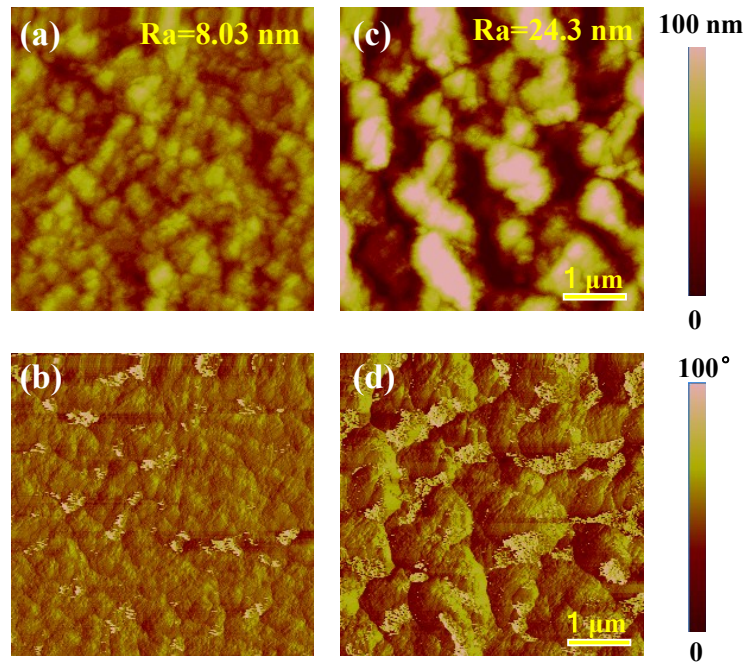


Figure S6. Surface morphology of P3CT-BN/P3HT bilayer coated perovskite (a-b) and P3HT coated perovskite (c-d) by AFM in tapping mode.

Table S2. Peak position of Pb at different depth of bare perovskite, P3CT-BN or P3HT covered perovskite.

Peak position of Pb (eV)	Surface	-10 nm	-20 nm
perovskite	138.35	138.72	138.80
perovskite/P3CT-BN	138.81	138.84	138.81
Perovskite/P3HT	138.75	138.74	138.81

Table S3. Peak position of I at different depth of bare perovskite, P3CT-BN or P3HT covered perovskite.

Peak position of I (eV)	Surface	-10 nm	-20 nm
perovskite	619.24	619.61	619.69
perovskite/P3CT-BN	619.67	619.7	619.7
Perovskite/P3HT	619.66	619.67	619.72

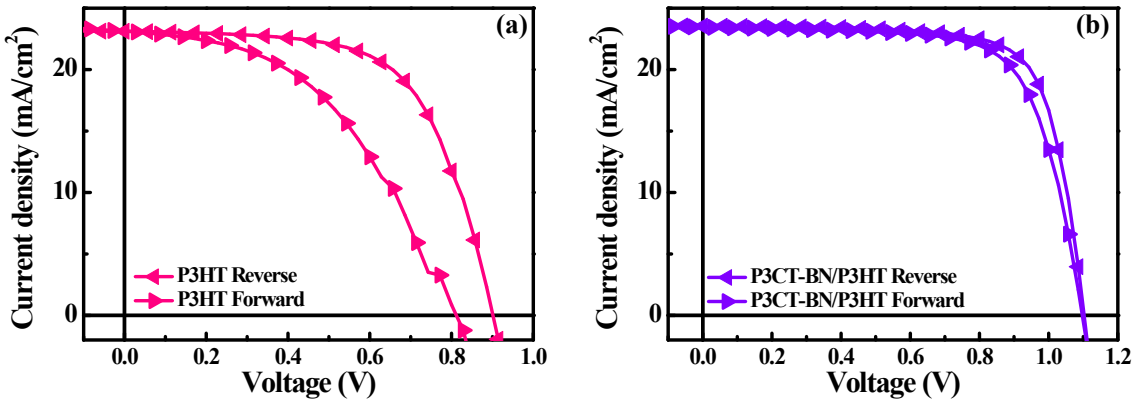


Figure S7. J-V curves at both forward and reverse scans collected under AM 1.5 simulated sunlight for P3HT based devices with (a) and without P3CT-BN buffer layer (b).

Table S4. Detailed parameters of the champion P3HT based cells with and without P3CT-BN buffer layer at forward and reverse scan.

Cells	Scan direction	V_{oc} (V)	J_{sc} (mA cm^{-2})	FF (%)	PCE (%)

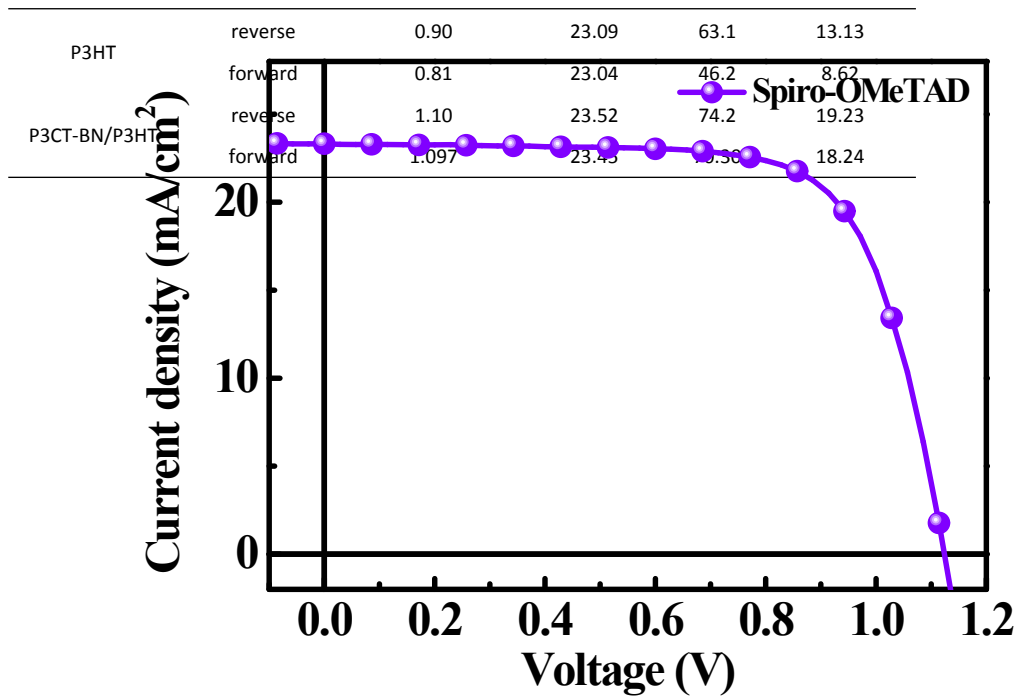


Figure S8. J-V scan characteristic of perovskite solar cells using doped Spiro-OMeTAD HTL.

Table S5. Parameters of the TRPL spectroscopy based on the glass/perovskite, perovskite/P3HT, perovskite/P3CT-BN and perovskite/P3CT-BN/P3HT, respectively.

Samples	Tave (ns)	τ_1 (ns)	A1	τ_2 (ns)	A2
glass/perovskite	622	65	0.31	650	0.62
glass/perovskite/P3HT	424	17.68	0.32	432	0.67
glass/perovskite/P3CT-BN	295	12.76	0.41	303	0.61
glass/perovskite/P3CT-BN/P3HT	200	5.58	0.42	205	0.57

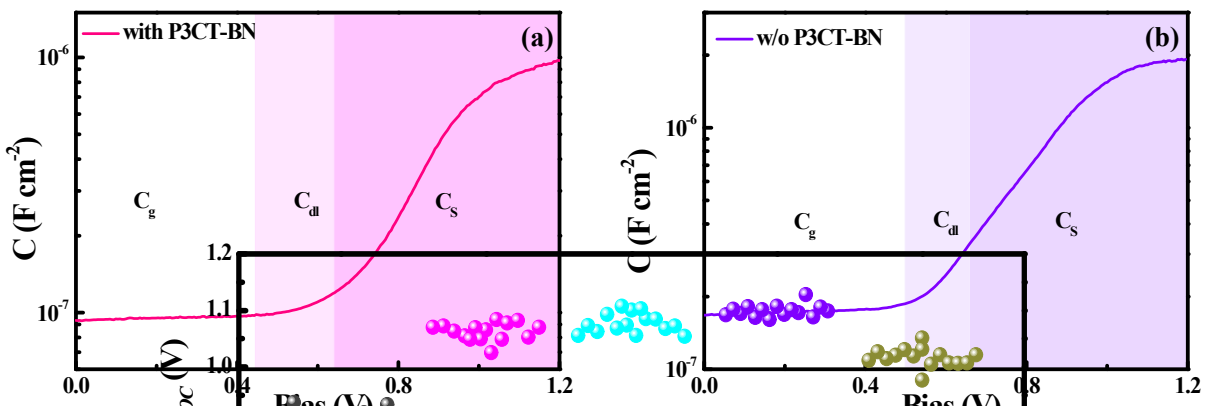


Figure S10. Illustrative of respective capacitance-voltage curves of Mott-Schottky plots for P3HT based PSCs with and without P3CT-BN interlayer. And three voltage regions can be differentiated allowing for correct MS analysis.

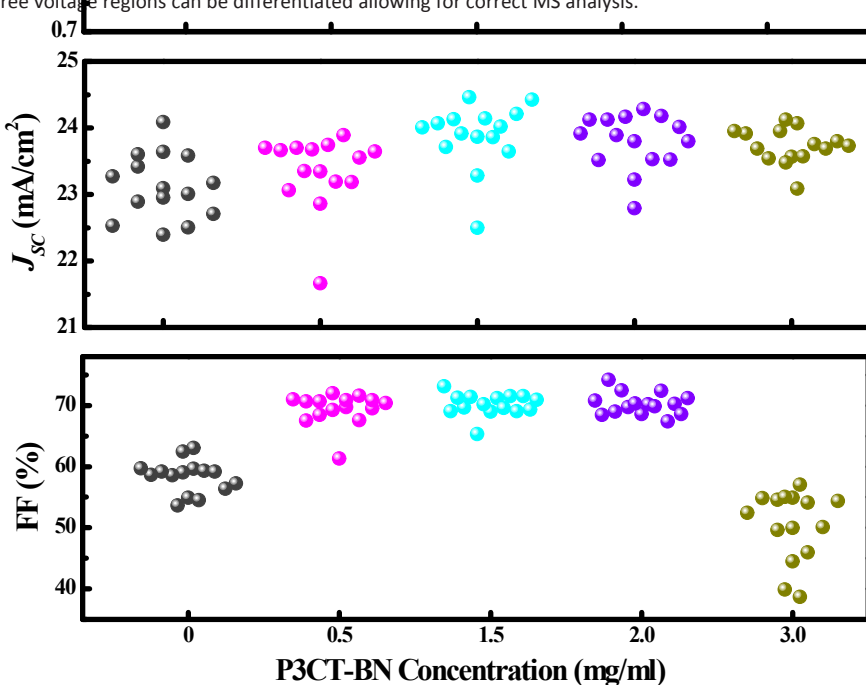


Figure S9. Statistical parameters of 15 devices based on P3CT-BN/P3HT HTL with different interlayer thickness.

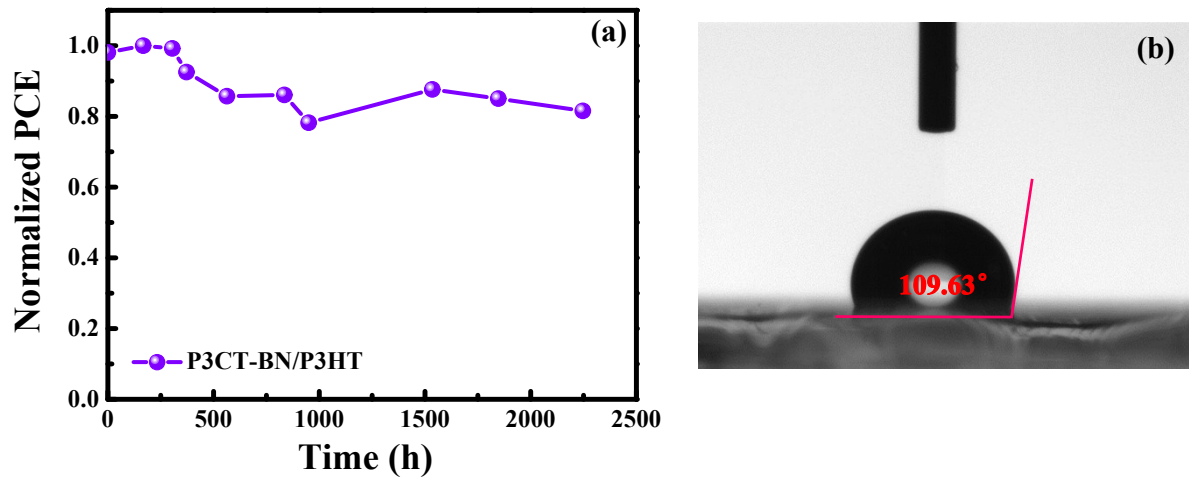


Figure S11. (a) Stability of P3CT-BN/P3HT based PSCs in air atmosphere with 50% humidity. (b) Contact angles between perovskite/P3CT-BN/P3HT and water.

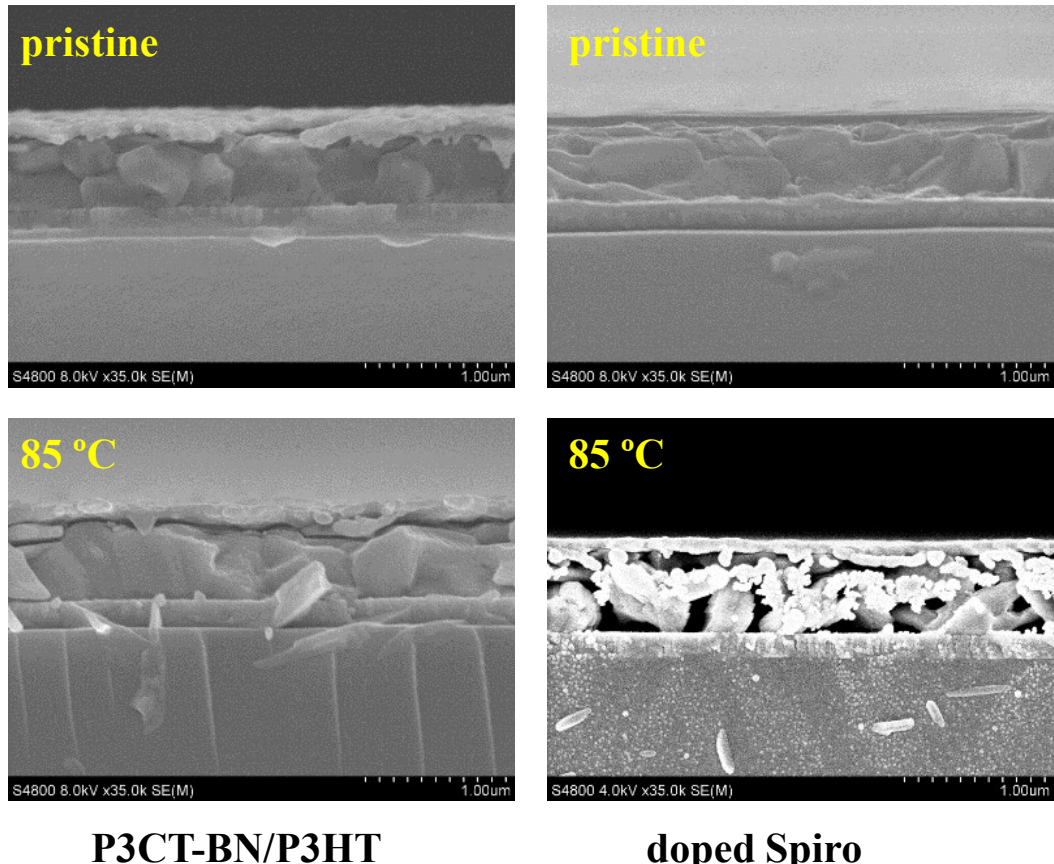


Figure S12. The cross-section SEM image of devices based on P3CT/P3HT (a-b) and doped Spiro-OMeTAD (c-d) HTL before and after heating at 85 °C in N₂ for 96 h.

References

- [1] J. Zhang, T. Zhang, L. Jiang, U. Bach, & Y. B. Cheng, *ACS Energy Lett.* 2018, **3**, 1677-1682.
- [2] N. Y. Nia, F. Matteocci, L. Cina, & D. A. Carlo, *ChemSusChem* 2017, **10**, 3854-3860.
- [3] Q. Hu, E. Rezaee, Q. Dong, H. Shan, Q. Chen, L. Wang, B. Liu, J.-H. Pan, Z.-X. Xu, *Sol. RRL* 2019, **3**, 1800264.
- [4] Y. Yue, N. Salim, Y. Wu, X. Yang, A. Islam, W. Chen, J. Liu, E. Bi, F. Xie, M. Cai, L. Han, *Adv. Mater.* 2016, **28**, 10738-10743.
- [5] J.Y. Seo, H. S. Kim, S. Akin, M. Stojanovic, E. Simon, M. Fleischer, A. Hagfeldt, S. M. Zakeeruddin, M. Gratzel, *Energy Environ. Sci.* 2018, **11**, 2985-2992.
- [6] Y. Guo, C. Liu, K. Inoue, K. Harano, H. Tanaka, E. Nakamura, *J. M. Chem. A*, 2014, **2**, 13827-13830.
- [7] S. N. Habisreutinger, T. Leijtens, G. E. Eperon, S. D. Stranks, R. J. Nicholas, H. J. Snaith, *Nano Lett.* 2014, **14**, 5561-5568.
- [8] M. Cai, V. T. Tiong, T. Hreid, J. Bell, H. Wang, *J. Mater. Chem. A* 2015, **3**, 2784-2793.
- [9] J. Xiao, J. Shi, H. Liu, Y. Xu, S. Lv, Y. Luo, D. Li, Q. Meng, Y. Li, *Adv. Energy Mater.* 2015, **5**, 1401943.
- [10] J. Ye, X. Li, J. Zhao, X. Mei, Q. Li, *RSC Adv.* 2016, **6**, 36356-36361.
- [11] J. W. Jung, J.-S. Park, I. K. Han, Y. Lee, C. Park, W. Kwon, M. Park, *J. Mater. Chem. A* 2017, **5**, 12158-12167.
- [12] M. Ahmadi, Y. C. Hsiao, T. Wu, Q. Liu, W. Qin, B. Hu, *Adv. Energy Mater.* 2017, **7**, 1601575.
- [13] Y. Zhang, M. Elawad, Z. Yu, X. Jiang, J. Lai, L. Sun, *RSC Adv.* 2016, **6**, 108888-108895.
- [14] T. Gatti, F. Lamberti, P. Topolovsek, M. Abdu-Aguye, R. Sorrentino, L. Perino, M. Salerno, L. Girardi, C. Marega, G. A. Rizzi, M. A. Loi, A. Petrozza, E. Menna, *Sol. RRL* 2018, **2**, 1800013.
- [15] M. Ulfa, T. Zhu, F. Goubard, T. Pauperté, *J. M. Chem. A*, 2018, **6**, 13350-13358.
- [16] P. Zhou, T. Bu, S. Shi, L. Li, Y. Zhang, Z. Ku, Y. Peng, J. Zhong, Y.-B. Cheng, F. Huang, *J. Mater. Chem. C* 2018, **6**, 5733-5737.
- [17] J. Y. Kim, G. Kwak, Y. C. Choi, D.-H. Kim, Y. S. Han, *J. Ind. and Eng. Chem.* 2019, **73**, 175-181.
- [18] N. Yaghoobi Nia, E. Lamanna, M. Zendehdel, A. L. Palma, F. Zurlo, L. A. Castriotta, D. A. Carlo, *Small*, 2019, **15**, 1904399.
- [19] F. Qi, X. Deng, X. Wu, L. Huo, Y. Xiao, X. Lu, A. K. Y. Jen, *Adv. Energy Mater.* 2019, **9**, 1902600.